Local Dynamics of Carbohydrates. 1. Dynamics of Simple Glycans with Different Chain Linkages

Angelo Perico,[†] Michele Mormino,[†] Ranieri Urbani,[‡] Attilio Cesàro,[‡] Emmanuel Tylianakis,[§] Photis Dais,[§] and David A. Brant*,[||]

Istituto di Studi Chimico-Fisici di Macromolecole Sintetiche e Naturali, Consiglio Nazionale delle Ricerche, via De Marini, 6, I-16194 Genova, Italy, Dipartimento di Biochimica, Biofisica e Chimica delle Macromolecole, Università di Trieste, I-34127 Trieste, Italy, Department of Chemistry, University of Crete, 71409 Iraklion, Crete, Greece, and Department of Chemistry, University of California, Irvine, California 92697-2025

Received: January 4, 1999; In Final Form: July 19, 1999

The present work gives the preliminary results of a systematic theoretical investigation of the relationship of structure and dynamics for a series of naturally occurring carbohydrate polymers as a function of the topological features, i.e., sugar composition and linkage type. Specifically, homopolymeric (1→3)- and (1→4)-linked α- and β-D-glucans and homopolymeric (1→4)-linked α- and β-D-galactans are considered. These polysaccharide chains cover a broad spectrum of macromolecular stiffness and extension. The theoretical calculations are developed within a diffusive approach that takes accurately into account the polymer connectivity and the corresponding conformational energy surface. This theoretical approach to the polymer dynamics, designated as the optimized Rouse Zimm local dynamics (ORZLD) theory, has been improved and implemented for applications to random coil polysaccharides in solution. The results show that correlation times, such as those obtainable from appropriate NMR, fluorescence, radiation scattering, and rheological relaxation experiments, are very sensitive to the details of the molecular structure and reveal patterns that are useful for characterizing the different chain topologies. Correlations are also illustrated among the dynamic chain pattern (i.e., the position and chain length dependence of the correlation times), equilibrium chain stiffness parameters, and the primary structure of the chain.

1. Introduction

An understanding of the three dimensional shapes of oligo- and polysaccharide chains and the dynamic characteristics of these chains is essential in order to interpret their biological functions as well as to control and improve their properties for industrial applications in the food, biomedical, textile, and paper industries. The physico-chemical properties and functions of carbohydrate polymers (e.g., efficiency in perturbing aqueous solution viscosity, ability to form gels, viscoelastic properties in the sol and gel states, thermal stability, etc.) are directly related to the details of the conformational space accessible to these polymers and the time-dependent transformations among the accessible conformational states. Various experimental probes of the conformation and dynamics of macromolecules are available, among which magnetic resonance,[1] fluorescence,[2] and dynamic scattering,[3] have been extensively explored. In comparison, a theoretical description based on realistic chain models has been afforded only to a very limited extent.

Recent theoretical progress in polymer dynamics, based on a diffusive approach which takes into account polymer connectivity together with an accurate description of the accessible conformational space, put local dynamics on a well founded molecular basis. This approach, designated the optimized Rouse−Zimm local dynamics (ORZLD) theory,[4] has been improved and implemented for application to random coil polysaccharides in solution. It is subject to comparison with systematic observations of static and dynamic properties over wide ranging scales of length and time. The theoretical approach can be designed to incorporate the structure of the polysaccharide chain at various levels of detail. The appropriate level of detail clearly depends on the frequency range of the motions under consideration.

Linear homopolysaccharides, differing from one another only in glycosidic linkage position and stereochemistry, can display a wide range of equilibrium conformational features.[5,6] Well-known equilibrium conformational differences of glucans are schematically illustrated by the stiff and extended (1→4)-β-linked chain of cellulose,[7,8] the "pseudo-helical" (1→4)-α-linked random coil chain of amylose[9] or by the disordered open helical motif of the (1→3)-β-linked chain of curdlan.[6,10] The time dependence of the conformational changes in solution is likely also to be dependent on the features of the glycosidic linkages.[11−13] These local motions are conveniently measured by the spectral density of $^{13}C-^{1}H$ bond motions in the nanosecond frequency range, as has already been done for oligodextrans and oligoamyloses.[11,12]

A project is currently underway in our laboratories to develop a structural understanding of the conformational mobility and dynamics of oligo- and polysaccharides in solution. Possible correlations between the conformational dynamics and the structural details are sought. The present work gives the initial results of a systematic theoretical investigation of the structure−dynamics relationships for a series of naturally occurring sugar sequences. Specifically, homopolymeric (1→3)- and (l→4)-α-

* To whom correspondence should be addressed. Telephone: (949) 824-6019. Fax: (949) 824-8571. E-mail: dbrant@uci.edu.
[†] Istituto di Studi Chimico-Fisici di Macromolecole Sintetiche e Naturali.
[‡] Dipartimento di Biochimica.
[§] Department of Chemistry, University of Crete.
[||] Department of Chemistry, University of California.

10.1021/jp990034x CCC: $18.00
Published on Web 09/08/1999

and β-linked D-glucans and homopolymeric (1→4)-α- and β-linked D-galactans are considered. These six chains encompass a wide spectrum of behavior with respect to chain trajectory and extension,[6] and it is therefore of interest to compare their respective dynamic characteristics as predicted by the ORZLD approach. In a forthcoming paper,[14] experimental results obtained with two different series of glucan oligomers containing (1→4)-α and (1→6)-β linkages are compared with theoretical predictions using several levels of complexity for the two chain models.

Before entering into a description of the methods used here, we present some general aspects of the conformational description of polysaccharides in their random coil solution state. The early free rotation approximations[15−17] have been improved with the introduction of the rotational isomeric state approach.[18,19] Interdependence of the backbone torsional angles of a given glycosidic linkage is taken routinely into account, but the assumption of mutual independence of the successive glycosidic linkages is often justified by the spatial separation provided by the nearly rigid intervening sugar residues.[7,20] Configuration-dependent properties of polysaccharides are calculated from models that incorporate a realistic geometric description of the molecular structure and a realistic approximation to the conformational potential energy surface for representative skeletal segments.

The potential energy surface may be estimated at several levels of approximation. The surface is typically a potential of mean force (pmf) in a highly restricted "soft" coordinate space, which often includes explicitly only the polysaccharide linkage torsion angles. The surface may be obtained most readily using simple molecular mechanics assuming a single rigid mean sugar residue geometry and constancy of all structural variables except the linkage torsion angles.[7,21,22] More realistic approximations allow the residue geometry to relax for each choice of linkage torsion angles,[23] or they use molecular dynamics or Monte Carlo simulations to generate pmfs in linkage torsion angle space averaged over all other motions of the polymer chain.[24] Solvent may be included in the latter approach with considerable additional commitment of computing resources.[25] For many purposes it is sufficient to use the more primitive approximations to the pmf, and this is often justified in particular by the paucity of experimental data appropriate for testing a given approximation.

Because there exist at present very few experimental conformational dynamics data with which to compare the results of the present ORZLD calculations, it is prudent to proceed in the present instance using potential energy surfaces estimated in the least expensive way. Within this "rigid residue" level of approximation we are then able to investigate the dynamical consequences of variations in the stereochemistry of the glycosidic linkage. In this respect the calculations performed here to explore the conformational dynamics have their counterpart in earlier calculations of the equilibrium spatial properties already reported for the same polysaccharides.[6]

2. ORZLD Model for Chain Backbone Description of Polysaccharides

In this paper we will develop models for the six homopolysaccharides described above in order to study the correlations among polymer microstructure, chain flexibility and extension, and the local conformational dynamics.

The Reduced Coordinate Model with the Rigid Residue. In this section the specific reduced coordinate model is illustrated. The polymer chains have been treated in the approximation of independent glycosidic linkages,[7] so it is sufficient to consider only the representative dimeric segments of the chains and the corresponding interactions of the nearest neighbor pair of residues. The conformational interdependence has thus been confined to the torsional angles of each linkage. The skeletal sugar residues have been taken rigidly constrained to their most stable $^4C_1$ chair conformation, using averaged α-D-glucose residue coordinates found in the literature and previously used for the calculations of amylose aqueous solution properties.[26,27] All internal coordinates are fixed as the variables ϕ, ψ have been stepped incrementally in 10° intervals through the full angular range. Hydrogen bonding between sugar hydroxyl groups has been suppressed in an effort to approximate better the intrapolymer interactions in an aqueous environment.[28] The force field employed has been described previously.[29]

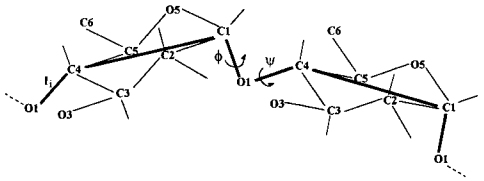

Figure 1. Definition of bond variables in the ORZLD calculation for the case $J = 4$. The chain backbone is made from chemical bond O1−CJ, virtual bond CJ−C1, and chemical bond C1−O1. The conventional O1-to-O1 virtual bond is not shown in the drawing.

In all cases the allowed conformational states are reported in terms of energy maps shown in the full $2\pi \times 2\pi$ space of the torsional variables ϕ and ψ for the glycan dimer in question. The torsion dihedral angles are defined as

$$\phi = \mathrm{H1-C1-O1-C}J'$$

$$\psi = \mathrm{C1-O1-C}J'\mathrm{-H}J'$$

where CJ' and HJ' are the carbon and hydrogen atoms of the reducing residue of the dimer. In the present case $J' = 3'$ or $4'$; prime marks designate atoms of the reducing residue. The signs of dihedral angles are taken according to the rules recommended by the IUPAC-IUB nomenclature.[30]

The polysaccharide chain backbone can be described by chemical and virtual bonds which connect the mass elements of the model (beads). The mass elements are either real atoms, simple united atoms (e.g., CH_2), or more complicated united atoms that may incorporate many atoms of a given sugar residue. Reduced coordinate models for the description of the sugar backbone are proposed here.

Polysaccharide chains are often represented in terms of virtual bonds that span (essentially) rigid sugar residues to link the oxygens of successive glycosidic linkages.[20] The chain model adopted here for the dynamic description uses three bond variables per conventional virtual bond (see Figure 1). Two of these bond variables coincide with the chemical bonds O1−CJ and C1−O1, and the third is a virtual bond connecting atom CJ to atom C1 ($J = 4$ in Figure 1). There is thus a total of $3N$ backbone bonds in a chain of N conventional virtual bonds or N sugar residues. These $3N$ bonds connect $n = 3N + 1$ mass points or beads. For a long chain approximately one-third of these beads are the oxygens of the glycosidic linkages, and the other two, centered on atoms CJ and C1, represent united atoms, each of which accounts for approximately half of the mass of a sugar residue. The specific partitioning of real atoms into the united atoms is given in Table 1. Partitioning the mass elements of the chain in this way is only a matter of convenience in the calculations and does not limit the meaning of the final results.

TABLE 1: Hydrodynamic Parameters for Mass Elements of the Model

united atom location, $J = 3$ or 4	net mass of united atom (g/mol)	effective radius of united atom (Å)	united atom frictional coefficient ξ_i at 22 °C (g/sec × 10^9)	heavy atoms included in united atom
O1	16	1.600	3.022	O1
CJ	87	2.750	5.193	C3, O3, C4, C5, C6, O6
C1	59	2.512	4.744	O5, Cl, C2, O2

Since the sugar ring is assumed rigid, the relative positions of the mass elements within a given sugar residue are constant.

The solvent viscosity required as a parameter of the calculation is that of water at 25 °C ($\eta = 0.8900$ cp). The frictional coefficient ζ_i of the mass elements that coincide with the glycosidic oxygens are obtained using Stokes' law and assuming that these oxygens are spherical with a radius equal to the tabulated van der Waals radius (1.6 Å). For the united atoms we estimate the surface area using the accessible surface area (ASA) method.[31] This surface is assumed to be spherical, and the frictional coefficient is estimated from Stokes' law in conjunction with the radius of the spherical united atom.

Molecular Modeling of the Local Dynamics of Realistic Polymeric Chains. A detailed description of the theory of the local dynamics in the ORZ approximation is given elsewhere;[2,4,32] a short presentation and discussion are reported here. The diffusional motions of a polymeric chain in dilute solution are responsible not only for the long range viscoelastic properties observed by low frequency oscillatory viscosity or dynamic light scattering experiments but also for the shorter scale dynamics probed by dielectric or NMR relaxation and fluorescence depolarization. For instance, it is known that the characteristic spin-lattice ^{13}C relaxation time T_1 from NMR relaxation experiments depends on the second-order time correlation function (TCF) $P_2(\theta(t))$, defined according to the relation[32]

$$P_2(\theta(t)) = 3/2\,\langle\cos^2(\theta(t))\rangle - 1/2 \tag{1}$$

where $\theta(t)$ is the angle through which the $^{13}C-H$ bond vector rotates in a time t.

In order to evaluate accurately the TCF $P^i{}_2(t)$ and the corresponding correlation time τ^i for a bond vector $\mathbf{l}_i$, a detailed description of the actual intramolecular potentials of the polysaccharide chain is required. In this paper, the polysaccharide chain is represented as a sequence of $n - 1 = 3N$ bonds joining n beads with friction coefficients ζ_i at the spatial positions $\mathbf{R}_i$. The coordinates $\mathbf{R}_i$ are considered as the set of slow variables characterizing the configuration time evolution in a hydrodynamic model for the solvent. The motion of the polysaccharide is described by a generalized diffusion equation here expressed in the equivalent generalized Langevin equation (GLE) form[33]

$$\frac{\partial \mathbf{R}_i}{\partial t} + \sigma \sum_{j=0}^{n-1} (\mathbf{HA})_{ij}\mathbf{R}_j(t) + \sum_{j=0}^{n-1} \int_0^t \mathbf{K}_{ij}(t-\tau)\cdot\mathbf{R}_i(\tau)\,\mathrm{d}\tau = \mathbf{v}^*_i(t) \tag{2}$$

The optimized Rouse−Zimm (ORZ) approximation to the GLE neglects the memory functions $\mathbf{K}_{ij}(\tau)$, thereby converting eq 2 to the ORZ Langevin dynamics[4,33,34]

$$\frac{\partial \mathbf{R}_i(t)}{\partial t} + \sigma \sum_{j=0}^{n-1} (\mathbf{HA})_{ij}\mathbf{R}_j(t) = \mathbf{v}^*_i(t) \tag{3}$$

Here $\mathbf{v}^*_i(t)$ are the Gaussian random velocity fluctuations with the correlation function

$$\langle \mathbf{v}^*_i(t)\cdot\mathbf{v}^*_j(t')\rangle = (6k_BT/\zeta)\mathbf{H}_{ij}\delta\,(t-t') \tag{4}$$

H and **A** are the preaveraged hydrodynamic interaction and structural matrices, respectively,

$$\sigma = 3k_BT/l^2\zeta \tag{5}$$

is the bond rate constant with

$$l^2 = (n-1)^{-1}\sum_{i-1}^{n-1}\langle l_i^2\rangle \tag{6}$$

the mean-square length of the vector bond defined as

$$\mathbf{l}_i = \mathbf{R}_i - \mathbf{R}_{i-1} \tag{7}$$

and

$$\zeta = n^{-1}\sum_{i=0}^{n-1}\zeta_i \tag{8}$$

the mean friction coefficient.

Matrix **A** of order n is given in terms of the inverse **U** of the normalized static bond correlation matrix

$$\mathbf{U}^{-1}_{ij} = \langle \mathbf{l}_i\cdot\mathbf{l}_j\rangle/l^2 \tag{9}$$

as

$$\mathbf{A} = \mathbf{M}^T\begin{pmatrix}0 & 0\\ 0 & \mathbf{U}\end{pmatrix}\mathbf{M} \tag{10}$$

The bead to bond vector transformation matrix **M** is a function of the topology of the chain,[2,35] and for linear chains it has the form

$$\mathbf{M} = \begin{pmatrix} \frac{1}{n} & \frac{1}{n} & . & . & . & \frac{1}{n} \\ -1 & 1 & 0 & \cdot & . & 0 \\ 0 & -1 & 1 & 0 & . & 0 \\ . & . & . & . & . & \cdot \end{pmatrix} \tag{11}$$

Matrix **H** is the equilibrium average of the dimensionless Oseen hydrodynamic interactions

$$\mathbf{H}_{ij} = (\zeta/\zeta_i)\{\delta_{ij} + \zeta_r(\zeta_i/\zeta)\,\langle l/R_{ij}\rangle\,(1-\delta_{ij})\} \tag{12}$$

The averaged overall hydrodynamic strength, defined exactly by

$$\zeta_r = \zeta/6\pi\eta_0 l \tag{13}$$

is assigned the value 0.25, which is considered appropriate for ordinary polymers in ideal solution.[36,37] Note that the theory is independent of the average quantities l and ζ but depends on the individual l_i and ζ_i.

The molecular modeling requires the equilibrium averages $\langle \mathbf{l}_i\cdot\mathbf{l}_j\rangle$ and $\langle 1/R_{ij}\rangle$ which are defined in general by the equilibrium distribution function

$$\psi_{eq}(\{\mathbf{R}_i\}) = \exp(-V(\{\mathbf{R}_i\})/k_BT)/\int \mathrm{d}\{\mathbf{R}_i\}\,\exp[-V(\{\mathbf{R}_i\})/k_BT] \tag{14}$$

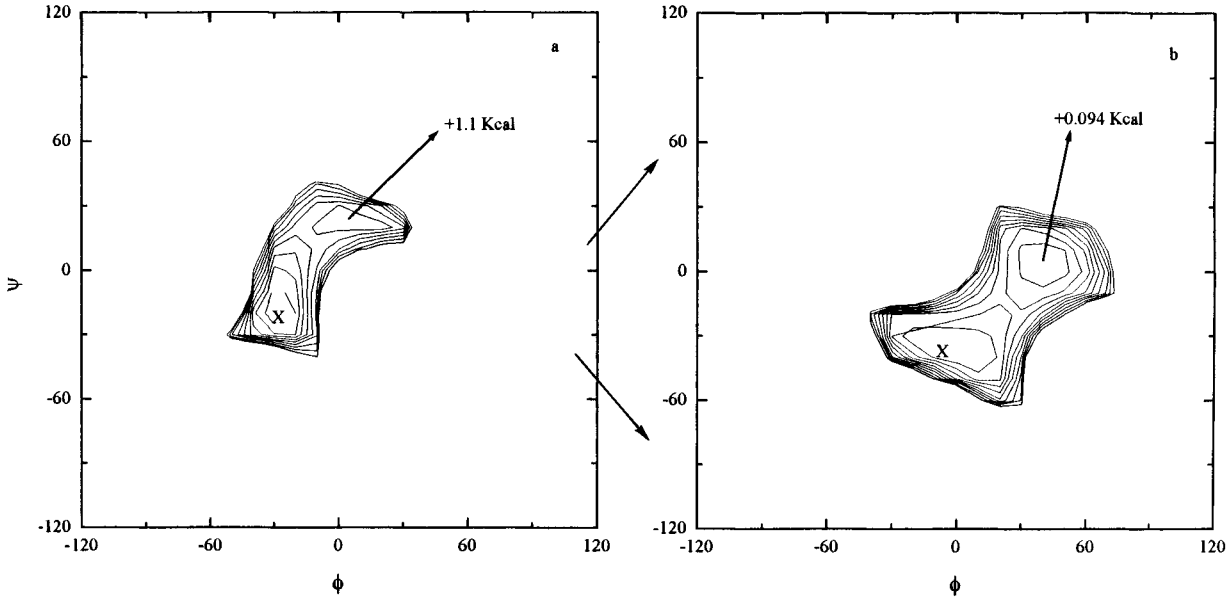

Figure 2. Conformational energy maps for (a) the α(1→4)glc dimeric unit and (b) the β(1→4)glc dimeric unit.

obtaining

$$\langle \mathbf{l}_i \cdot \mathbf{l}_j \rangle = \int \mathrm{d}\{\mathbf{R}_i\} \psi_{\mathrm{eq}}(\{\mathbf{R}_i\})(\mathbf{l}_i \cdot \mathbf{l}_j) \tag{15}$$

$$\langle 1/\mathbf{R}_{ij} \rangle = \int \mathrm{d}\{\mathbf{R}_i\} \psi_{\mathrm{eq}}(\{\mathbf{R}_i\})(1/\mathbf{R}_{ij}) \tag{16}$$

where $V(\{\mathbf{R}_i\})$ is the intramolecular potential of mean force.

In the ORZ approximation the dynamic properties are sensitive to the evaluation of the individual friction coefficients and to the accuracy of the description of the atomistic intramolecular potential. The second-order orientational relaxation of any bond $\mathbf{l}_i$ is given by eq 1, which may be equivalently written as

$$\mathrm{P}_2^i(t) = \frac{2}{3}\langle [\mathbf{l}_i(t) \cdot \mathbf{l}_i(0)]^2 / l_i^2(t) \cdot l_i^2(0) \rangle - \frac{1}{2} \tag{17}$$

It may be calculated exactly according to the ORZLD theory and turns out to be[32]

$$\mathrm{P}_2^i(t) = 1 - 3\{x^2 - x^3(\pi/2)[1 - (2/\pi) \arctan x]\} \tag{18}$$

with

$$x = [1 - (M^i(t))^2]^{1/2}/M^i(t) \tag{19}$$

Here the fundamental TCF $M^i(t)$ of bond vector $\mathbf{l}_i$ is defined as

$$M^i(t) = \langle \mathbf{l}_i(t) \cdot \mathbf{l}_i(0) \rangle / \langle l_i^2 \rangle \tag{20}$$

and has the exact ORZLD form

$$M^i(t) = \sum_{a=1}^{n-1} (Q_{ia} - Q_{i-1a})^2 \mu_a^{-1} \exp(-\sigma \lambda_a t) \tag{21}$$

Here $\mathbf{Q}$ and $\{\lambda_a\}$ are the eigenvectors and eigenvalues of the product matrix $\mathbf{HA}$ while μ_a, which indicates the inverse of the normalized mean-square length of the mode a, is the diagonal element a of the diagonal matrix $\mathbf{Q^T AQ}$. Note that, in the case of rigid bonds in a residue or of parallel bonds in the chain, singularities arise in the matrix $\mathbf{U}^{-1}$, but the eigenvalue problem can still be solved in terms of the inverse of $\mathbf{HA}$, after taking care of the translational eigenvalue.[38] Finally the correlation time τ^i of the TCF $\mathrm{P}^i{}_2(t)$, the experimental orientational relaxation time, has the form

$$\tau^i = \int_0^\infty P_2^i(t)\, \mathrm{d}t \tag{22}$$

3. Conformational Energies and Equilibrium Averages

Figures 2−4 show the pertinent portions of the energy contour maps for the homopolymeric (1→4)- and (1→3)-α- and β-linked D-glucans and homopolymeric (1→4)-α- and β-linked D-galactans with contour level stepped by 0.5 kcal/mol from 0 to 5 kcal/mol above the energy minimum, which is marked on the map by the cross symbol. The relative energies of the important subsidiary minima are also indicated on the maps.

The conformational energy surfaces of the polymers considered here have been used to compute certain average configurational properties of the unperturbed chain, namely, the mean square unperturbed end-to-end distance $\langle r^2 \rangle_o$, the characteristic ratio

$$C_N = \langle r^2 \rangle_o / N l_\nu^2 \tag{23}$$

the persistence length

$$P_N = \langle (\mathbf{l}_1 \cdot \mathbf{R}_{0N}) \rangle / l_1 \tag{24}$$

the equilibrium bond vector correlation matrix $\mathbf{U}^{-1}$, and the matrix of the mean inverse distances $\langle 1/R_{ij} \rangle$. The latter quantities are required as input into eqs 9 and 12 of the dynamic theory and are related, respectively, to the structural features of the chain and the Oseen hydrodynamic interaction matrices. Here N is the number of sugar residues, and l_ν^2 is the mean-square length of the conventional glycosidic oxygen-to-glycosicidic oxygen virtual bond. Following the usual definitions,[20] the characteristic ratio of eq 23 is normalized by the mean-square end-to-end length of a freely jointed chain of N conventional virtual bonds. An alternative definition normalizes the mean-square end-to-end distance by the mean-square length of the bonds of the chain model l^2 times the total number of bonds thus giving

$$C_n = C_N(l_\nu^2/l^2)[N/(n-1)] \tag{25}$$

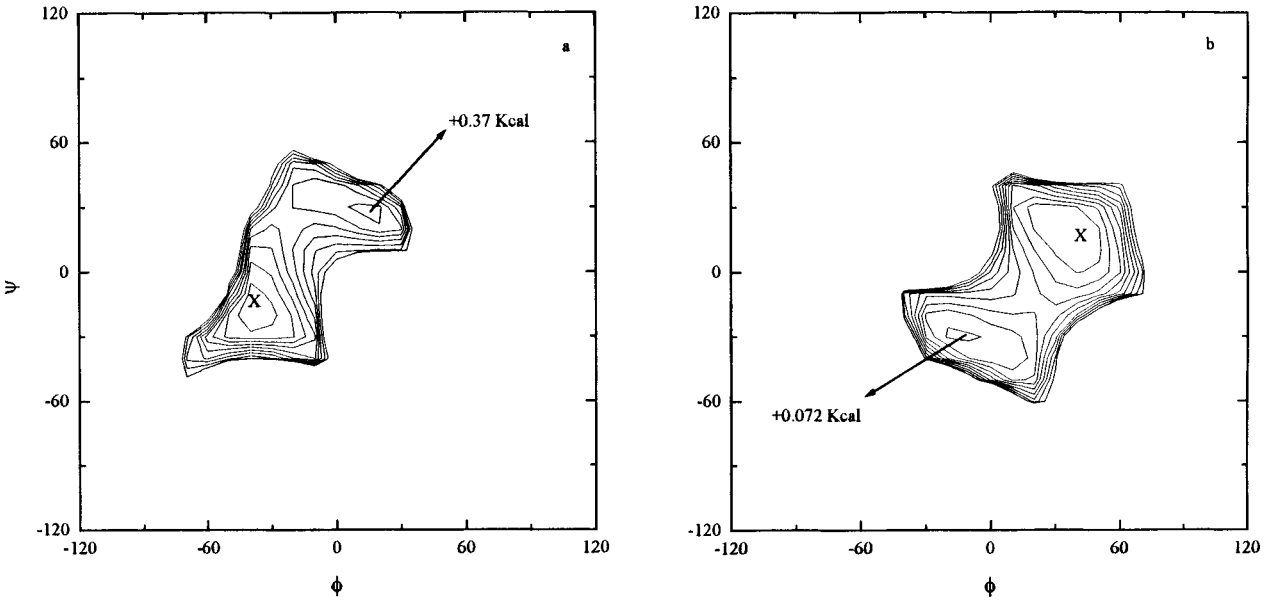

Figure 3. Conformational energy maps for (a) the α(l→3)glc dimeric unit and (b) the β(1→3)glc dimeric unit.

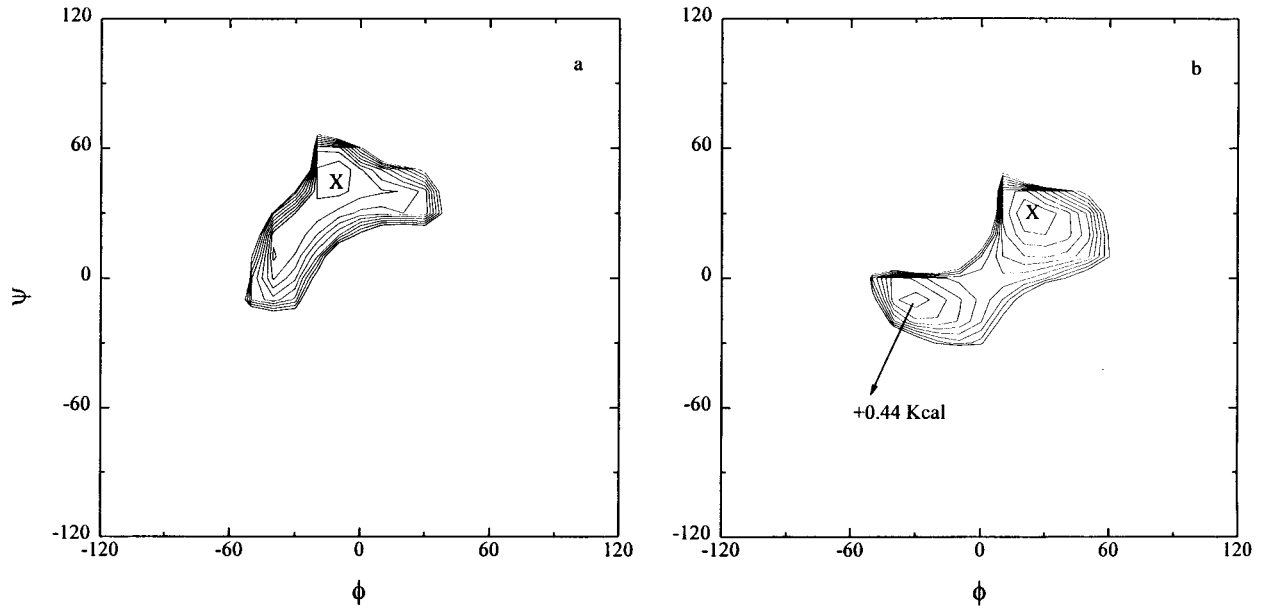

Figure 4. Conformational energy maps for (a) the α(l→4)gal dimeric unit and (b) the β(1→4)gal dimeric unit.

It is evident that the two definitions provide the same information, but C_n should be preferred for comparing polymers of very different virtual bond length l_v and a very similar mean-bond length l as in the case of the (1→4)-α- and β-linked D-galactans (see Figures 14 and 15, below, and the related discussion).

The equilibrium averages have been estimated by using the method of Monte Carlo chain generation together with the approximation of separable configuration energy.[9] In this method, for a given degree of polymerization N and temperature, polymer chains are grown in the computer to create an ensemble of chains (from 10^5 to 10^6 chains) with a distribution of configurations consistent with the particular choice of energy surface in the ϕ, ψ torsional angle space of the representative disaccharide.

A description of the relative extension of the polysaccharide chains is given in Figures 5 and 6, where the dependence of the characteristic ratio C_N on N is reported for the different glycosidic linkages. Similar trends are obtained for the persistence lengths P_N. The chain extension for long chains, as measured by C_∞, spans approximately 2 decades, from about 2.5 for the (1→3)-β-linked D-glucan (β(1→3)glc) to about 250 for the (1→4)-α-linked D-galactan (α(1→4)gal). Intermediate values are obtained for the (1→4)-β-linked D-galactan (β(1→4)-gal), the (1→4)-α-linked D-glucan (α(1→4)glc), the (1→3)-α-linked D-glucan (α(1→3)glc), and the (1→4)-β-linked D-glucan (β(1→4)glc). Thus, the polymer chains explored here display a large range of chain extension. The characteristic ratio C_N for the three more compact chains shown in Figure 5 are all close to their asymptotic limit C_∞ for $N = 100$. For the more extended chains described in Figure 6 C_N is still increasing strongly with N for $N > 100$. We emphasize that not all of the values of C_∞ computed here have been confirmed experimentally but the present calculations are believed to reflect the differences in chain extension in a qualitatively correct way.

Further insight into the equilibrium features of the different polysaccharides may be obtained by looking at local persistence lengths[4,39] and at the directional correlation between the bond vectors.[6] The local persistence length was quantitatively intro-

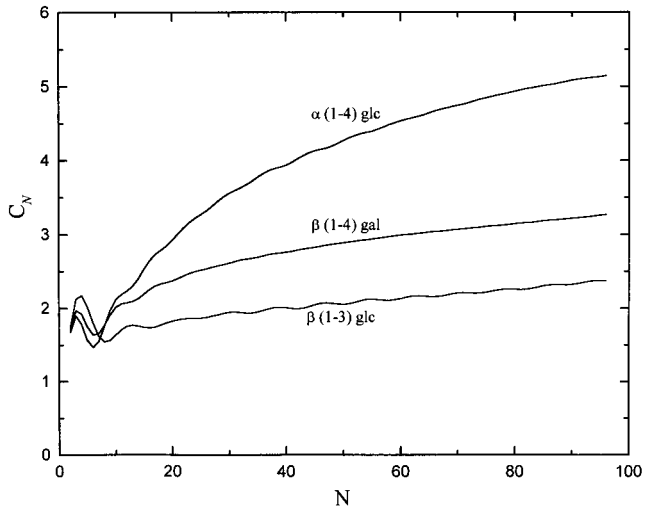

Figure 5. The characteristic ratios C_N for α(1→4)glc, β(1→4)gal, and β(1→3)glc as a function of the number of residues *N*.

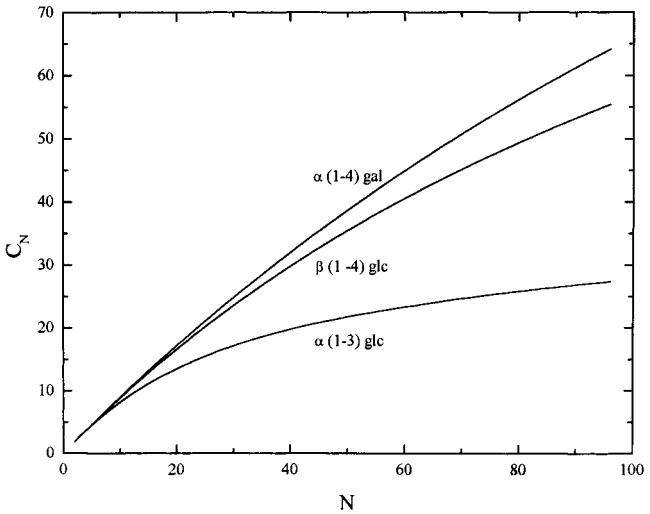

Figure 6. The characteristic ratios C_N for α(1→4)gal, β(1→4)glc, and α(1→3)glc as a function of the number of residues *N*.

duced[39] as the portion of the end-to-end distance statistically aligned with a given bond:

$$p_n^i/l = \sum_{j=1}^{n} \langle \mathbf{l}_i \cdot \mathbf{l}_j \rangle / l^2, \quad \{i = 1, ..., n\} \tag{26}$$

Here the local persistence length is defined for each bond in the chain of *3N* bonds and is normalized to the mean square backbone bond length l^2 defined in eq 6. It is soon recognized that the average local persistence length is identical to C_n of eq 25. The mean projection of the virtual bond in the center of the chain on each virtual bond *i* of the sequence

$$F_{N/2}^i = \langle \mathbf{l}_{\nu,N/2} \cdot \mathbf{l}_{\nu,i} \rangle / l_\nu^2 \tag{27}$$

is a descriptor of the structure of the chain, particularly describing the emergence of superresidue order or secondary (helical) structures. It is the same as the directional correlation function introduced earlier,[6] except that the central virtual bond is chosen to define the reference direction rather than a terminal virtual bond. The quantities p^in/l and $F^i{}_{N/2}$ will be discussed in the following section in connection with a description of the dynamic pattern of the different polymers.

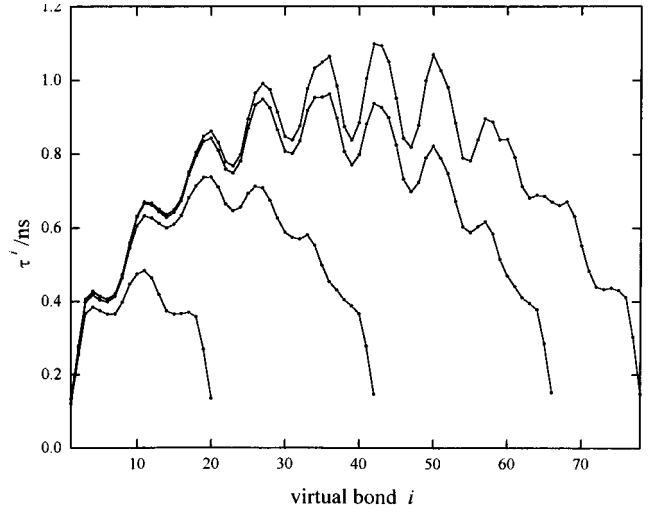

Figure 7. The dependence of τ^i on sequential position i for α(l→4)-glc for $N = 20, 42, 66, 78$.

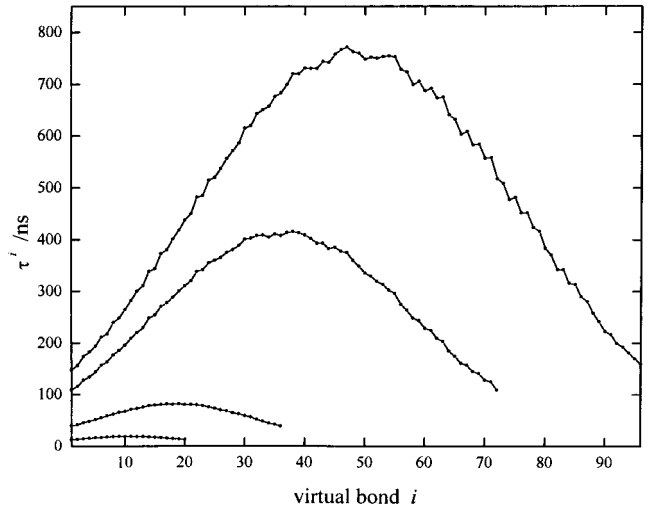

Figure 8. The dependence of τ^i on sequential position i for β(1→4)-glc for $N = 20, 36, 72, 96$.

Other assumptions about the basic structural model and potential functions would have led to some differences in the numerical values reported here. Our purpose, however, is to explore the *comparative* dynamic behavior of the six polysaccharide hompolymers considered. Significant differences described below, and the correlations found between dynamic behavior and the structural features of the chains, appear clearly to override artifacts that might arise from the relatively simple models employed.

4. Calculated Dynamic Properties

The second-order orientational correlation time τ^i of eq 22 has been calculated for each of the $n - 1$ bonds in the model (Figure 1) and for each of the conventional glycosidic oxygen-to-glycosidic oxygen virtual bonds for the several glycosidic linkages and for various chain lengths.

In Figures 7−12 the virtual bond dynamic patterns for the six polymers at different *N* values are reported. As expected, all the curves have an overall bell shape, which reflects a greater mobility of chain elements near the chain ends than those in the middle of the chain. In addition there are no particular domains of flexibility, which, on the other hand, is the typical fingerprint of heteropolymers like, for example, proteins.[2,38] The greatest slowing of the fluctuations, i.e., the largest τ^i values, is

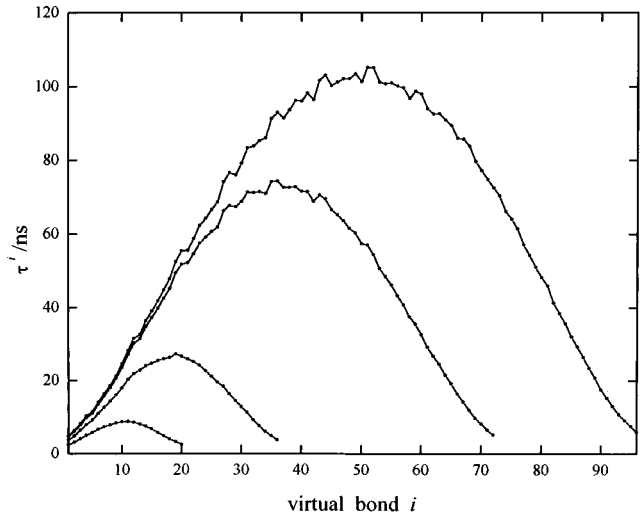

Figure 9. The dependence of τ^i on sequential position i for α(1→3)-glc for $N = 20, 36, 72, 96$.

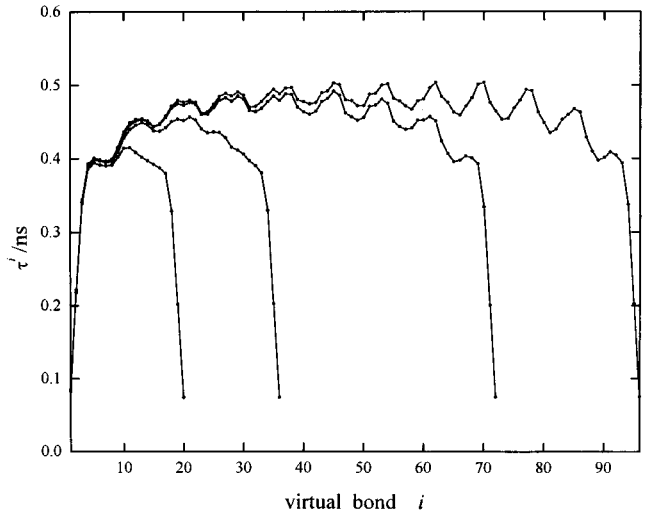

Figure 10. The dependence of τ^i on sequential position i for β(1→3)-glc for $N = 20, 36, 72, 96$.

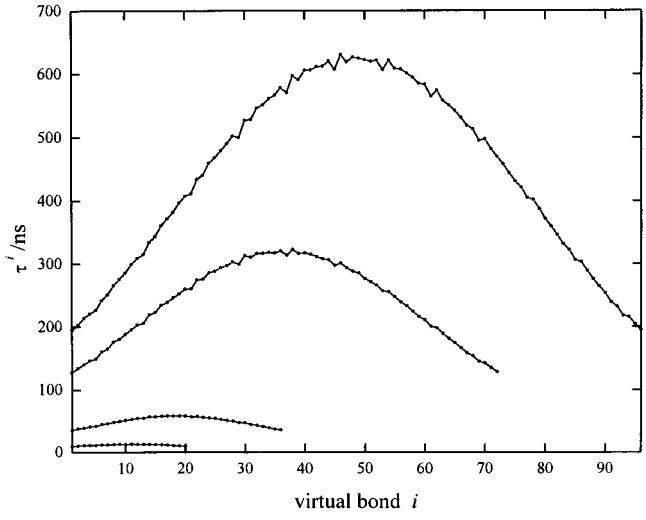

Figure 11. The dependence of τ^i on sequential position i for α(l→4)-gal for $N = 20, 36, 72, 96$.

found to be around the central residue. Going either to increasing values of *i* (the location of the bond) to the right, or to decreasing values of *i* (left), the general trend is for τ^i to become smaller as one approaches the chain terminus. At the chain ends the

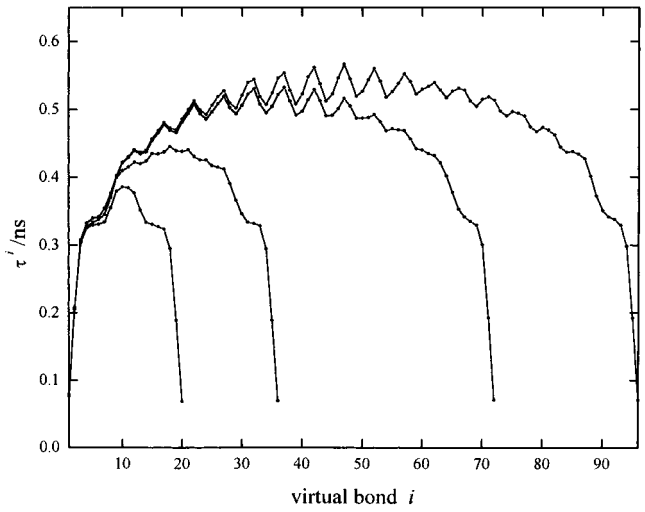

Figure 12. The dependence of τ^i on sequential position i for β(1→4)-gal for $N = 20, 36, 72, 96$.

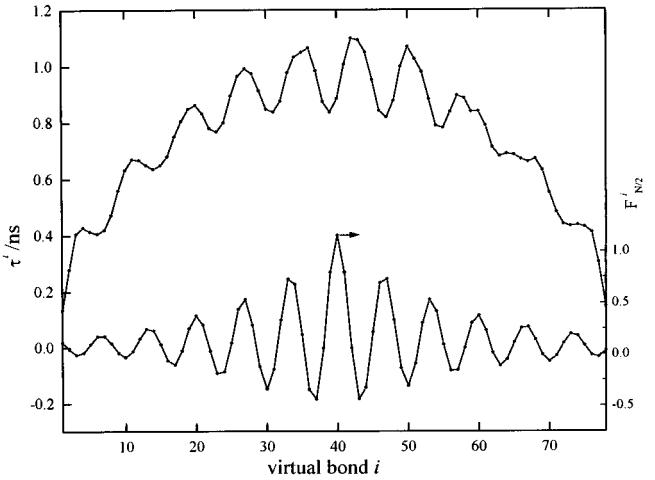

Figure 13. Comparison of the dependence of τ^i (upper curve) and $F^i_{N/2}$ (lower curve) on sequential position i for α(1→4)glucan with $N = 72$.

motional freedom is greatest, because residues (virtual bonds) are tied into the chain on only one side. The terminal residues are always more "mobile", irrespective of the particular chain geometry. The dynamical patterns should be nearly symmetric in our chain models with respect to the central residue. Perfect symmetry is not to be expected, however, since polysaccharide chains have a well-defined polarity inherent in their chemical structure.

In the cases of the α(1→4)glc (Figure 7), β(1→3)glc (Figure 10), and β(1→4)gal (Figure 12) chains, characteristic periodic undulations are observed in the variation of τ^i with *i*. In Figure 13 it is shown for α(1→4)glc (and similar results, not reported here, are obtained also for the other two chains) that the periodic undulations in τ^i in Figure 7 with a periodicity of 7−8 residues are directly correlated to those of the equilibrium bond correlation function $F^i_{N/2}$, the chain structure descriptor of eq 27, which is an indicator of the pseudo-helical structure of the polymer. The correlation of equilibrium ($F^i_{N/2}$) and dynamic (τ^i) chain descriptors clearly arises from incorporation of the equilibrium structural characteristics of the chain into the calculation of the correlation times through the equilibrium averaged matrices **U** (eq 9) and **H** (eq 12). The periodic oscillations in τ^i with *i* cannot, however, possess physical reality and must be a manifestation of approximations in the computations of equilibrium statistical averages incorporated in the theory. The TCFs

from which the τ^i values are computed are averaged over all orientations of a local, polymer-based coordinate system in the laboratory frame and over all internal motions of the polymer in the local frame. Hence, for the homopolymers under consideration, all identical virtual bonds far from the chain ends must behave identically with respect all physical properties and must display identical orientational dynamics. The artifactual oscillations are, in any case, of small amplitude relative to the dynamic range of the i dependence of τ^i shown in Figures 7−12, and we are inclined to believe this is a minor defect in the present theoretical description of the chain dynamics.

For three of the polymers described in Figures 7−12 the dynamic range of the position dependence of τ^i increases with the length of the chain in the range of the number of residues considered here. This effect is strongest for the polymers for which C_N is increasing with N throughout the range of DP investigated, i.e., polymers for which C_N is far from the asymptotic limit C_∞, as may be confirmed in Figures 5 and 6. In general, the stronger the increase in C_N with N, the greater the dynamic range of the position dependence of τ^i. The strongest exception to this sort behavior of τ^i is for the $\beta(1\rightarrow3)$-glc polymer (Figure 10), for which τ^i for interior residues approaches an asymptotic limit for modest values of N. Correspondingly, C_N (Figure 5) quickly reaches the asymptotic limit as N increases. According to the present conformational description this polymer is the most dynamically flexible of those compared here, even though some pseudo-helical structure is displayed (Figure 10).

The asymptotic behavior of τ^i predicted for the $\beta(1\rightarrow3)$glc oligomers in Figure 10 is characteristic of what is to be expected of all six of these chains, once they achieve sufficient length. In the case of $\beta(1\rightarrow3)$glc the local dynamic behavior of the interior residues has essentially converged for chains with DP = 50 or greater. Terminal units, and those near the termini, move more freely regardless of the DP of the chain, but one sees from Figure 10 that units embedded more than 25 units into the $\beta(1\rightarrow3)$glc chain are dynamically indistinguishable from other interior units. This is consistent with the observation that τ^i for interior residues is effectively independent of i for DP = 50 or more. The characteristic correlation length or wavelength of the local segmental motions of $\beta(1\rightarrow3)$glc is thus suggested to be somewhere around 25 residues. This prediction of the theory should be subject to confirmation with appropriate measurements on oligomeric chains. The rigid residue approximations used here to estimate the pmf surfaces for the representative dimeric segments may have the effect of overestimating the correlation lengths of the segmental motions of the six polysaccharides under consideration here, but the comparative behavior should be qualitatively accurate.

In general we observe that asymptotic behavior of the local dynamics of the central residues will occur in any chain for which the DP exceeds the correlation length of the segmental motions by a factor of about 2 or more. The local correlation times are sensitive to the correlation length, which increases with the stiffness of the chain. If the chain is significantly longer than this correlation length, addition of further units does not affect the local dynamics of central units of the chain. If the chain is shorter than the correlation length, the local dynamic pattern changes with the number of residues, and τ^i increases with increasing DP. This correlation length thus defines the meaning of local (segmental) motion. The greater the flexibility of the chain, the shorter the correlation length and the more local the segmental motion. Above a limiting DP, however, local dynamics and long range, global, dynamics (as obtained from intrinsic viscosity) become separable. On the contrary, for chains that are short compared to the local correlation length, long range motions and local motions are not easily resolved, and both contribute to the orientational dynamics of a given bond or virtual bond vector. In any case, end effects, arising from higher terminal unit mobility, are always detected, so that even short chains do not behave as a rigid body.

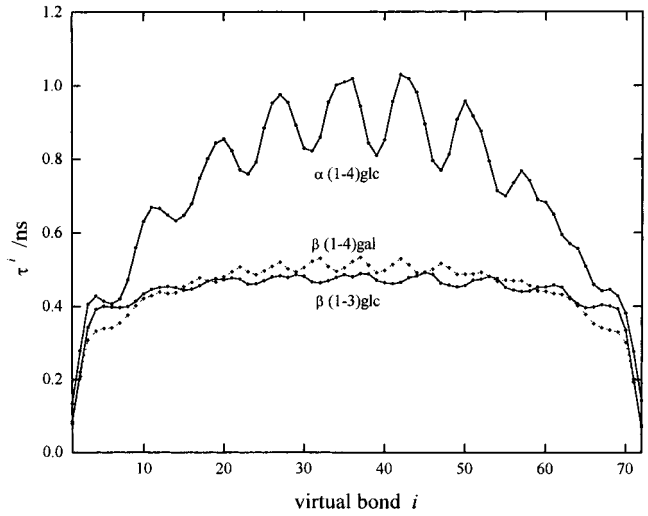

Figure 14. A comparison of the dependence of τ^i on sequential position i for $\alpha(1\rightarrow4)$glc, $\beta(1\rightarrow4)$gal, and $\beta(1\rightarrow3)$glc for $N = 72$.

These observations can also be cast in the language of the Rouse−Zimm (RZ) theory. For the smaller oligomers all of the modes in the RZ relaxation spectrum contribute to determine the values of the local bond correlations times τ^i. As the chain length grows, the slower, longer wavelength RZ modes undergo an increase in relaxation time, but they continue to contribute to the τ^i, and consequently the τ^i values grow with increasing chain length. (On the other hand, the fast, short wavelength RZ modes, which are more strongly coupled to the details of the local polymer structure, are much less sensitive to the DP of the oligomer.) Once the chain length is large enough, the relaxation times of the longer wavelength RZ modes become too slow to influence appreciably the correlation times τ^i characterizing the dynamics of the local motion of central residues. At this point the central residue τ^i values are dictated entirely by the characteristics of the local segmental motion, and the dynamical behavior of these residues becomes asmyptotic with increasing chain length. Under the same conditions, the τ^i for terminal or near-terminal residues also achieve asymptotic values, which are, however, shorter than those for the interior residues, because the flexible chain structure dictates that not even the shortest oligomers behave as rigid bodies. The terminal residues are never as encumbered by the sluggishness of the rest of the chain as are the interior residues.

Figures 14 and 15 compare the virtual bond dynamic patterns of the 6 polymers at $N = 72$. Because the correlation times span 2 orders of magnitude, the presentation has been split into two figures. Figure 14 reports the faster dynamics and Figure 15 the slower. The corresponding characteristic ratios C_n and C_N are reported for $N = 72$ in Table 2. As can be seen, the local dynamics are quite sensitive to the microstructure of the polysaccharide which in turn determines the extension of the chain. With inconsequential exceptions, the more extended the chain as measured by C_n, the longer the corresponding correlation times. Consider, for example, $\beta(1\rightarrow4)$glc and $\alpha(1\rightarrow4)$gal in Figure 15, where throughout most of the range of i the value of τ^i for $\beta(1\rightarrow4)$glc ($C_N = 46$, $C_n = 111$) is larger than that for

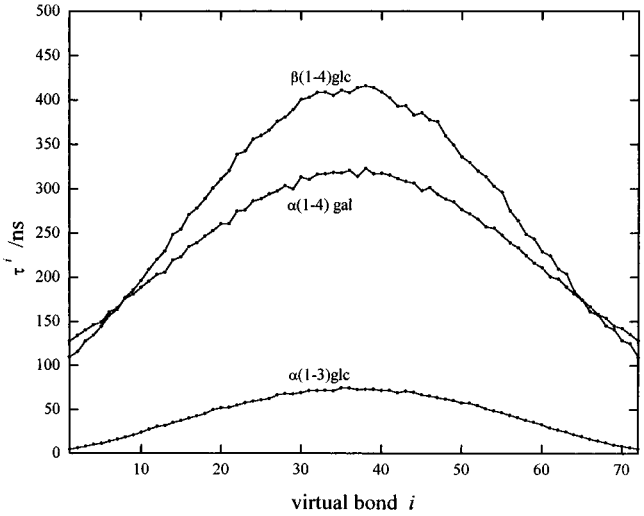

Figure 15. A comparison of the dependence of τ^i on sequential position i for β(1→4)glc, α(1→4)gal, and α(l→3)glc for $N = 72$.

TABLE 2: Characteristic Ratios C_N and C_n For $N = 72$

Polymer	l_v	C_N	l	C_n
α(1→4)glc	4.29	4.78	2.04	7.05
β(1→4)glc	5.47	45.9	2.03	111
α(1→3)glc	4.23	25.3	1.85	44.1
β(1→3)glc	4.76	2.22	1.86	4.85
α(1→4)gal	4.46	52.2	2.04	83.2
β(1→4)gal	4.18	3.08	2.04	4.31

α(1→4)gal ($C_N = 52$, $C_n = 83$) for $N = 72$. The dynamic pattern correlates with C_n but not with C_N, because C_n provides a more accurate gauge of the relative chain extension (or stiffness) than C_N.

It is important to observe at this point that the concept of dynamic flexibility, which has been invoked above, is a complex one that is related not only to the chain extension but also to the inherent conformational freedom of the backbone units of the chain and the detailed geometric structure of the of these units. This can be illustrated by a closer consideration of the conformational energy surfaces of several of these polymers. Figures 2 and 3 show that the conformational space accessible to the dimeric units of β(1→3)glc and β(1→4)glc is essentially identical. Hence, the local conformational freedom of these two polymers is very similar, and in this sense they share similar flexibililty. Yet the dynamic range of τ^i as a function of i is very different for the two chains, with the former apparently much more "flexible" as signified by the smaller virtual bond relaxation times and the shorter correlation length. Comparison of the α(1→4)glc and β(1→4)glc energy surfaces in Figure 2 shows that the former has considerably less local conformational freedom than the latter. Nevertheless, from the point of view of the magnitude and position dependence of τ^i, it is the α-(1→4)glc chain that appears to be the more "flexible". Thus, neither β(1→3)glc nor α(1→4)glc has greater inherent conformational freedom than β(1→4)glc, but they are more flexible by the dynamic criteria we have employed.

Since both the β(1→3)glc and α(1→4)glc are considerably more compact than β(1→4)glc, it is tempting to attribute the greater dynamic flexibility to the smaller coil dimensions and to assume that the overall rotations of the compact coil contribute to the rapid relaxation of local bond orientations. This is true, however, only for oligomers with chain lengths comparable to or less than the correlation length for segmental motions. For longer chains the overall motions of the coil are too slow to contribute significantly to local bond orientational relaxation, and the rates of relaxation of interior residues become independent of chain length. The common feature enjoyed by the fast-relaxing chains is, instead, the strong influence of glycosidic torsional motions ϕ and/or ψ on the orientation of the associated virtual bonds. Chains for which the virtual bond backbone trajectory changes abruptly with fluctuations in the glycosidic torsion angles are the ones which experience the most rapid relaxation of the local bond vector orientational correlations. These are precisely the chains that tend to display smaller overall chain extension, while it is the chains with stronger local directional persistence that display the greatest overall chain extension and the longer local bond relaxation times.

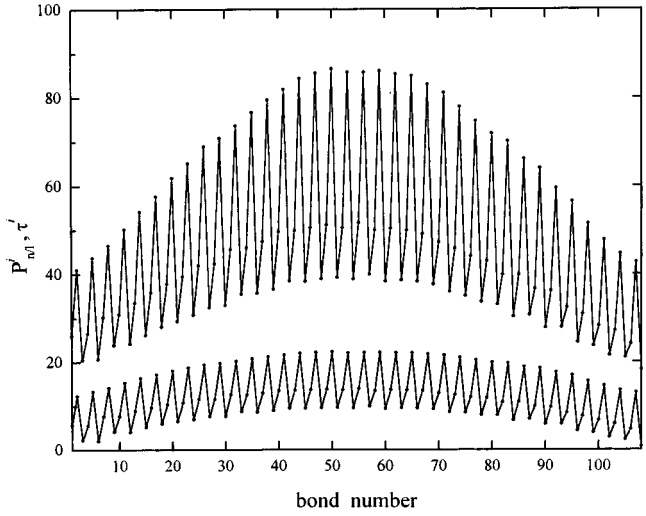

Figure 16. Correlation times τ^i (upper curve) and local persistence lengths p^i_n/l (lower curve) for the bonds of the model shown in Figure 1 for β(1→4)glc with $N = 36$ residues and $n = 108$ backbone bonds plotted as a function of the sequential position of the bond.

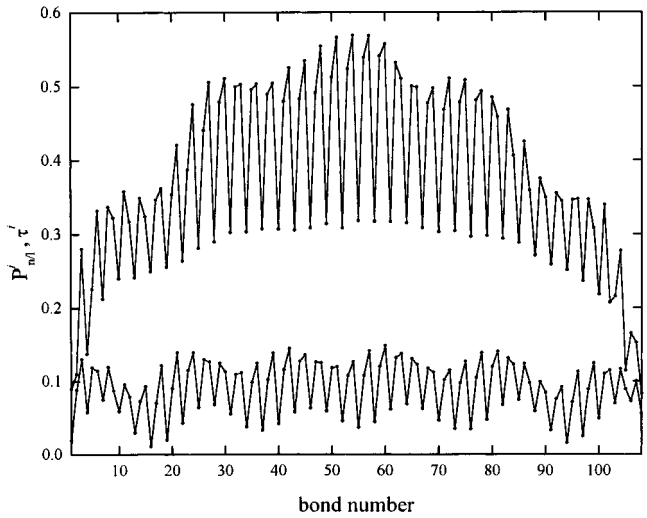

Figure 17. Correlation times τ^i (upper curve) and local persistence lengths p^i_n/l (lower curve) for the bonds of the model shown in Figure 1 for α(1→4)glc with $N = 36$ residues and $n = 108$ backbone bonds plotted as a function of the sequential position of the bond.

Finally we describe the effects of the three-dimensional structure of the residue on the dynamics. This point is addressed in Figures 16 and 17 for only two of the polymers; results for the others are similar. We report two curves in each figure, the upper curve representing the second order correlation time τ^i for the "bonds" of the model represented in Figure 1 and the lower curve the normalized bond persistence length p^i_n/l. In contrast to the periodic 6- to 8-fold oscillations seen in Figures 7, 10, and 12, the 3-fold oscillations in Figures 16 and 17 have

a solid physical basis. It can be seen that both static and dynamic curves show the same 3-fold periodicity, which arises from the presence of three bonds per repeat unit in the model employed. The spurious 6- to 8-fold oscillation can also be detected in Figure 17. The reasons for differences in the correlation times of the three bonds in a given repeat units are (1) that the three bond vectors have different mean orientations in the 3D structure of the unit relative to the local long axis of the chain and (2) that different masses (and frictional coefficients) are associated with the real and united atoms that constitute the "beads" in the chain. As illustrated by comparison of Figures 16 and 17 with Figures 7−12, ORZLD theory permits computation of relaxation times for real and/or virtual bonds of the chain, and the ultimate choice for comparison with experiment will be dictated by the nature of the experimental observables. It is moreover possible to model the chain to include not just one or three "bonds" per residue, but in as much realistic stuctural detail as desired or dictated by the nature of the experimental data.

5. Discussion and Conclusions

The present results can be generalised to other polysaccharides, although the details will depend on the particular features of the chain structure and the approximations of the model. The most obvious conclusion is that measurable local relaxation times τ^i are related strongly to the chain stiffness (or flexibility) but even more intimately to the topology and accessible conformational space of the polymer. In the polysaccharide oligomers and copolymers of greatest biological and commercial interest determinations of τ^i as a function of position in the chain can reveal the locations of greatest molecular mobility. It is necessary, however, to emphasize that the detailed dependence of τ^i on i predicted by calculations of the present sort may be difficult to observe experimentally, especially in homopolymers, because the resolution of experimental probes, e.g., ^{13}C NMR relaxation, may not permit differentiation among residues sharing similar ordinal positions in the chain. Thus, successful matching of theory with a limited range of observables may give confidence in further predictions of the theory not subject to experimental confirmation.

The results presented and discussed here show the considerable potential of the present theoretical approach for characterisation and interpretation of the dynamic conformational features of carbohydrates. In particular, it is important to observe that this approach avoids the arbitrary partition of molecular motions into separable fast and slow components that is so prevalent in current attempts to interpret the results of experimental dynamics measurements in biopolymer systems. A major virtue of the ORZLD approach is that the chain model can be constructed with as much realistic geometric detail as desired. As illustrated here, the full atomistic structure of the polysaccharide backbone units was included in computing the input matrix elements $\mathbf{U}^{-1}_{ij} = \langle \mathbf{l}_i \cdot \mathbf{l}_j \rangle / l^2$ and $\langle 1/\mathbf{R}_{ij} \rangle$. The model need not be restricted to the independent dimer and rigid residue approximations used here, and longer, more flexible elementary chain segments can be considered, if desired. The present focus on computation of τ^i for the conventional virtual bonds (Figures 7−12) and the more detailed three-bond representation of the sugar residues (Figures 16 and 17) was for purposes of illustration only. Correlation times, or directly observable NMR relaxation parameters such as NOE, T_1, and T_2, can also be calculated for specific $^{13}C-^{1}H$ bonds in the molecular structure, if such calculations are warranted by the available experimental data.

It is useful, finally, to mention that some underlying approximations of the present theoretical approach have recently been overcome[40] and that refinements of the theory can offer an even more reliable qualitative and quantitative description of the relationship between dynamics and conformational features of carbohydrate oligomers and polymers.

Acknowledgment. This work is supported in part by Progetto Strategico *Tecnologie Chimiche Innovative* by Progetto Coordinato *Sviluppo di algoritmi per il riconoscimento molecolare*, by Progetto Coordinato *Proprietà dinamiche di oligo e polisaccaridi* and Grant CT97.02765CT03 of the National Research Council of Italy, and by NIH Grant GM 33062.

References and Notes

(1) Peng, J.; Wagner, G. *J. Magn. Reson*. **1992**, *98*, 308−332.
(2) Hu, Y.; Fleming, G. R.; Freed, K. F.; Perico, A. *Chem. Phys*. **1991**, *158*, 395−408.
(3) Schmitz, K. S. *An Introduction to Dynamic Light Scattering by Macromolecules*; Academic Press: New York, 1990.
(4) Perico, A. *Acc. Chem. Res.* **1989**, *22*, 336−347.
(5) Rees, D. A. *Polysaccharide Shapes*; Chapman & Hall: London, UK.
(6) Burton, B. A.; Brant, D. A. *Biopolymers* **1983**, *22*, 1769−1792.
(7) Brant, D. A.; Christ, M. D. In *Computer Modeling of Carbohydrate Molecules*; French, A. D., Brady, J. W., Eds.; American Chemical Society: Washington, DC, 1990; Vol. 430, pp 42−68.
(8) Kroon-Batenburg, L. M. J.; Kruiskamp, P. H.; Vliegenthart, J. F. G.; Kroon, J. *J. Phys. Chem. B* **1997**, *101*, 8454−8459.
(9) Jordan, R. C.; Brant, D. A.; Cesàro, A. *Biopolymers* **1978**, *17*, 2617−2632.
(10) Kitamura, S.; Minami, T.; Nakamura, Y.; Isuda, H.; Kobayashi, H.; Mimura, M.; Urakawa, H.; Kajiwara, K.; Ohno, S. *J. Mol. Struct. (Theochem)* **1997**, *395*, 425−435.
(11) Kadkhodaei, M.; Wu, H.; Brant, D. A. *Biopolymers* **1991**, *31*, 1581−1592.
(12) Brant, D. A.; Liu, H.-S.; Zhu, Z. S. *Carbohydr. Res.* **1995**, *278*, 11−26.
(13) Brant, D. A. *Pure Appl. Chem*. **1997**, *69*, 1885−1892.
(14) Manuscript in preparation.
(15) Benoit, H. *J. Polym. Sci.* **1948**, *3*, 376−388.
(16) Eliezer, J.; Hayman, H. J. G. *J. Polym. Sci*. **1957**, *23*, 387−402.
(17) Burchard, W. *Makromol. Chem*. **1960**, *42*, 151−164.
(18) Flory, P. J. *Statistical Mechanics of Chain Molecules*; Wiley-Interscience: New York, 1969.
(19) Mattice, W. L.; Suter U. W. *Conformational Theory of Large Molecules*; John Wiley & Sons, Inc.: New York, 1994.
(20) Brant, D. A.; Goebel, K. D. *Macromolecules* **1975**, *8*, 522−530.
(21) Urbani, R.; Di Blas, A.; Cesàro, A. *Int. J. Biol. Macromol*. **1993**, *15*, 24−29.
(22) Brant, D. A. *Quart. Rev. of Biophys*. **1976**, *9*, 527−596.
(23) French, A. D.; Brady, J. W. In *Computer Modeling of Carbohydrate Molecules*; French, A. D., Brady, J. W., Eds.; ACS Symposium Series No. 430; American Chemical Society, Washington, DC, 1990; Chapter 1, pp 1−19.
(24) Schmidt, R. K.; Teo, B.; Brady, J. W. *J. Phys. Chem*. **1995**, *99*, 11339−11343.
(25) Ueda, K.; Brady, J. W. *Biopolymers* **1997**, *41*, 323−330.
(26) Goebel, C. V.; Dimpfl, W. L.; Brant, D. A. *Macromolecules* **1970**, *3*, 644−654.
(27) Brant, D. A.; Dimpfl, W. L. *Macromolecules* **1970**, *3*, 655−664.
(28) Stokke, B. T.; Talashek, T. A.; Brant, D. A. *Macromolecules* **1994**, *27*, 1124−1135.
(29) Urbani, R.; Cesàro, A. *Polymer* **1991**, *32*, 3013−3020.
(30) IUPAC-IUB Commission on Biochemical Nomenclature, *Arch. Biochem. Biophys*. **1971**, *145*, 405−436.
(31) Pastor, R.; Karplus, M. *J. Phys. Chem*. **1988**, *92*, 2636−2641.
(32) Perico, A.; Guenza, M. *J. Chem. Phys*. **1985**, *83*, 3103−3109.
(33) Zwanzig, R. *J. Chem. Phys*. **1974**, *60*, 2717−2720.
(34) Bixon, M.; Zwanzig, R. *J. Chem. Phys*. **1978**, *68*, 1890−1895.
(35) Guenza, M.; Mormino, M.; Perico, A. *Macromolecules* **1991**, *24*, 6168−6174.
(36) Perico, A.; Piaggio, P.; Cuniberti, C. *J. Chem. Phys*. **1975**, *62*, 4911−4918.
(37) Osaki, K.; Shrag, J.; Ferry, J. *Macromolecules* **1972**, *5*, 144−147.
(38) Perico, A.; Guenza, M.; Mormino, M.; Fioravanti, R. *Biopolymers* **1994**, *35*, 47−54.
(39) Perico, A. *Biopolymers* **1989**, *28*, 1527−1540.
(40) Perico, A.; Pratolongo, R. *Macromolecules* **1997**, *30*, 5958−5969.